Rim and tyre investigation for the in-wheel motor of an electric vehicle using simulations

A Kulkarni[a], and A Kapoor[a]

[a] *Faculty of Engineering and Industrial Science, John St Hawthorn Victoria-3122*
Email: ambarishkulkarni@swin.edu.au

Abstract: Global demands for sustainability and compelling requirements to reduce environmental impacts have greatly influenced the transportation industry to look into ways to reduce carbon emissions. In recent years, electric vehicle (EV) development has taken a new paradigm due to environmental pollution, global warming and depletion of fossil fuels. Unlike automobiles with internal combustion engines (ICEs), EVs have intrinsic advantage of zero emission during operation, when used with renewable energy source for charging batteries.

To date most of the commercial EVs use permanent magnet motors (PMMs) due to specific low weight, and compact size (as it relies on use of permanent magnets for magnetic path). The key disadvantage of PMM is the need for rare earth elements, which also influence costs. To overcome the cost and availability issues associated with PMM, a new material or motor type is required to sustain EV growth. In this research alternative in-wheel (series mounting arrangement) switch reluctance motor (SRM) is designed which is fitted to a small car. The in-wheel SRM is selected due to specific advantages, i) use of non-rare earth element for magnetic path (stators and rotors), ii) low transmission losses (increased energy efficiency as it is direct drivetrain), iii) simplifies the design due to redundancy of mechanical systems (packaging of gearboxes, differentials, drive shafts and axles are not required, thus reducing the weight, cost and space requirements), and iv) increased ground clearance (due to redundancy of gear boxes and drive shafts). Small car provided substantial advantages with light vehicle weight, low power requirements, and enough mud guard clearances to implement in-wheel SRM.

In a wheel, the rim has typically been designed as a cylindrical metallic component, functioning as holder between car chassis and tyres. Tyres were added onto the rim perimeter, as a link between roads and rims, providing required cushioning effect. Consequently, in-wheel SRM EV had the intrinsic advantage of direct drive. However, this design increased the overall mass, as the wheel required an appropriate rim-tyre construction. Moreover, the in-wheel design with an SRM added further weight at the rear of the vehicle, changing its dynamics and performance. In this research, different rim-tyre models were analysed in context of an in-wheel SRM for developing the customised rim design and tyre selection. The suitability of the rim-tyre based on an in-wheel drivetrain required performance simulation pertaining to loads and dynamics at tyre-road interface. The rim selection was based on finite element (FE) simulation of five different sets. The standards and regulations for producing passenger car wheels in Victoria, Australia, were studied and successfully implemented in the development phase of this study. This paper describes the rim-tyre study conducted for in-wheel SRM. Starting with the rim optimisation, an appropriate tyre based on low rolling resistance was selected. The development of the rim-tyre configuration of the in-wheel SRM featured:

- Designing a rim for an in-wheel SRM design based on low unsprung mass and appropriate space that can accommodate motor, focusing on the rim size, shape and materials.
- Optimising rim topology by comparing different types of rims based on low weight characteristics for thermal and deflection simulations, as well as following recommendations for “Rim & Tyre Standards-Australia”.
- Tyre selection that meets two main objectives—low road resistance and clearance with mudguards—as well as detailed character mapping simulations to determine the appropriate tyre for the in-wheel design.
- Designing motor-to-wheel attachments, whereby making the wheel an integral part does not affect maintenance.

Keywords: *EV, In-wheel motor, rims, tyres and simulations*

1. INTRODUCTION

In comparison to automobiles with internal combustion engines (ICEs), EVs have the intrinsic advantage of zero tail pipe emission during the operation, when a renewable energy source is used for charging batteries. There is an increasing acceptance of electric vehicles (EVs) as alternative sustainable vehicles based on four criteria, i) environmental issues, ii) government policies, iii) commercial viability, and iv) new technological opportunities. Environmental issues have encouraged government policies to subsidies green vehicle prices. A decade ago EVs were seen as impractical; however rising fuel prices have led to the commercial viability. These developments have created a new technological opportunity for all stake holders in the EV industry to develop an innovative automotive technology.

In this work, a small car Holden Barina Spark was used as a mule vehicle. The in-wheel drivetrain configuration selection for a selected Holden Barina Spark was based on the key criteria: i) minimal power transmission losses (maximising the motor power output), ii) independent control of wheels, and iii) simple design —as these were the key prerequisites for a success of the EV drivetrain. The EV drivetrain motor selection was based on the following objectives: i) power density, ii) weight, iii) cost, iv) maintenance, v) size and vi) speed/torque. The four main motor classifications compared for key desirables are: i) Bush Direct current motor (BDCM), ii) Induction motor (IM), iii) Permanent magnet motor (PMM), and iv) Switch reluctance motor (SRM). The BDCM has low power density, very high weight, very high maintenance, large size, and low speed/torque profile (Xue, Cheng et al. 2008). The IM has medium power density, large weight, moderate cost, and moderate maintenance, large size, and moderate speed/torque profile (Chan 2002, Xue, Cheng et al. 2008). PMM has been the best motor choice in terms of its high power density, low weight, small size, and low maintenance requirements. The cost of PMM is higher due to high arising price from demand of less abundant elements used in the construction of the motor magnetic path. Nonetheless, high costs due to scarcity of rare earth elements are still important concerns for PMM (Seaman 2010, Campbell August 2008). Based on objectives, the SRM was suitable for the in-wheel design (Wadnerkar, Tulsiram et al. 2005, Kulkarni, Kapoor et al. 2011).

This paper describes the modelling and the simulation of the rim-tyre for an in-wheel SRM. The wheel consists of a rim and a tyre. The rim provides the structural rigidity and tyre provides the vehicle traction as well as cushioning when the vehicle travels on uneven surfaces. The rim and the tyre are interdependent and work as a single component influencing the vehicle drive characteristic. In the wheel, a new proposed SRM adds an extra weight and thermal loads. Hence, the structural performance of the rim is even more crucial, As a consequence five rim topologies were modelled for an optimisation using finite element (FE) methods . The approporiate rolling resistance tyre dictates an increase in the EV range. Hence the tyre was modelled for examining the rolling resistance performance and longitudinal slip. In this research the rim and tyre were evaluated for an in-wheel SRM EV with following objectives:

- Compliance to “Rims and Tyre standards-Australia 2010” for an appropriate rim and tyre nomenclature and material selection. Key factors affecting the rim design are weight, rigidity, durability, and thermal stability. The weight optimisation was done on five rims (topologies) to select an appropriate rim based on structural rigidity, thermal stability, and life cycle assessment. The FEM was used to acess these criteria.
- To increase the EV range by selecting an appropriate rolling resistance tyre and modelling the longitudinal slip variation for comparison between an ICE Holden Barina Spark tyre with an in-wheel SRM Holden Barina Spark tyre.

2. RIM DEVELOPMENT

2.1. Rim nomenclature

Motor power output is dependent on the rim size and the shape. The rim-tyre nomenclature defines rim shapes and sizes. In the Australia, the rim and the tyre conform to “Rims and Tyre standards-Australia 2010”, which provides basic dimensions for the rim diameter, width, and flange shape. Using the clearance and fitment to selected Holden Barina Spark a suitable 205J50 R17 rim-tyre was selected.

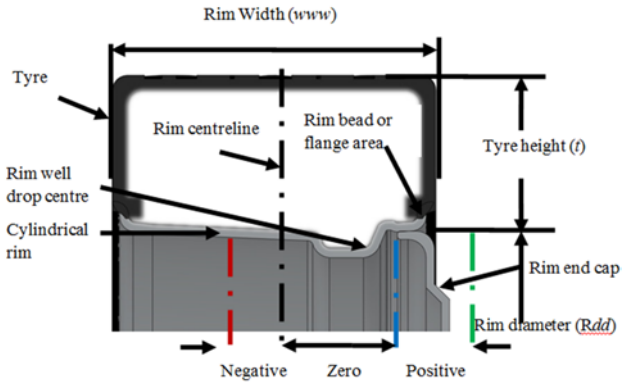

Figure 1. Rim nomenclature

The rim topology consists of a cylindrical rim and a cross sectional web (also called end cap) supporting it as shown in Figure 1. The rim and the end cap is constructed as: i) a single piece, ii) two-piece, and iii) three-piece.

The end cap is offset to the rim centerline (as shown in Figure 1) and based on the offset, rim is classified as: i) zero (i.e. from the center black line to the blue line), ii) positive (i.e. from the green line to the blue line), and iii) negative (i.e. from the centre black line to the red line). In the negative offset rim, end cap is closer to rim back side, hence motor space becomes small. For this reason, the negative offset rim is not considered in this research. The end cap construction uses supports to provide the structural rigidity to the rim. Following are typical end cap supports used in this research: i) solid, ii) hollow (shown in Figure 3), iii) three support, and iv) five support.

2.2. Finite element modelling

The rim is an integral part of the new proposed SRM. The SRM adds extra mass and thermal loads to the rim. The available off the shelf rim is not suitable as the end cap offset may not provide adequate motor space and is also heavier. The design objective was to have a light weight rim, which provided a maximum motor space. Figure 2 depicts the FE method flow diagram used for the rim optimisation in this research. To achieve the objectives, five rim designs were modelled. An example of rim 3, a two piece rim with a positive offset using a hollow end cap was modelled (referred to as rim 3). The rim 3 weighed 7kg in total and had eight bolt holes near the cylindrical rim as shown in Figure 3. The bolt holes were near the cylindrical rim on the end cap face. It was seam welded between the cylindrical rim and the end cap.

The FE models were developed for all five rim topologies in the Ansys test bench 13.1. Initially, each rim was modelled using the local and the global 3D tetrahedral mesh with 4 nodes. The valve hole, bolt holes, and rim perimeter faces were modelled with a local tetrahedral finer mesh of 1 to 3mm. The global tetrahedral mesh of 6mm or more was modelled into the rest of the rim with smooth transition ratio of 0.272.

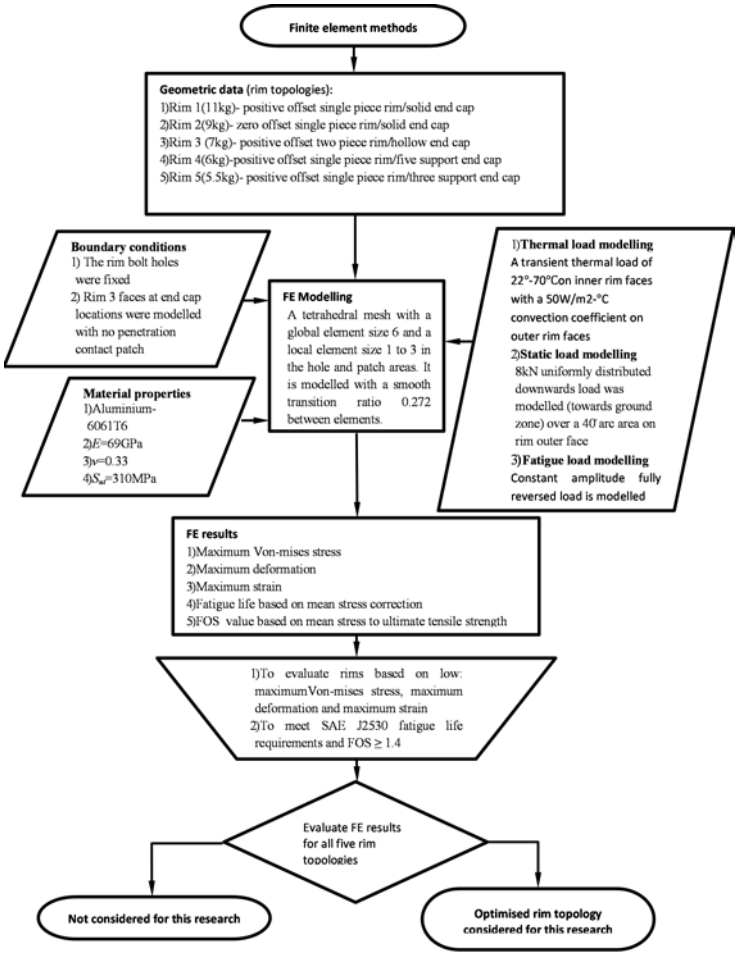

Figure 2. *Rim optimisation flow diagram using FE methods*

Figure 3. Rim 3 model

2.3. Material and boundary conditions

Rim material was selected as the Aluminium spun rim had following advantages over the other alloys: i) structural rigidity - good, as the Aluminium alloy 6061 T6 has a 340MPa material yield strength (Merlin, Timelli et al. 2009), ii) thermal stability - good, as they possesses the low elongation percentage when compared to other grades of Aluminium, iii) manufacturing defects- good, as it is spun it has no porosity defects (e.g.: die cast alloys), iv) weight- medium due to the density of Aluminium, and v) cost-medium, as they are relatively cheaper than the magnesium and the carbon fibre material. The aluminium 6061 T6 spun material was modelled into all five FE rim models with: i) Young's modulus (E) 69GPa, ii) Poisson's ratio (ν) 0.33, iii) coefficient of thermal expansion (α) 23.6X10-6/°C and iv) density (ρ) 2.7g/cc.

In the FE method the boundary conditions are modelled to simulate the physical conditions of the rim. In a car, the rim is restrained for rotational and translation movements to the chassis at the bolt holes location as shown in Figure 4. This was achieved by effectively modeling fixed restrains on bolt holes within the FE model. Further the contact patches were modelled in FE environment to establish the working relation within multi body parts. As shown in Figure 4, only the rim 3 was modelled with the no penetration contact patch (as others were single piece) between the rim and end cap faces.

2.4. Load conditions

Figure 4 is an example of the rim 3, which summarises loads modelled as: i) the thermal load, ii) the static load, and iii) the fatigue load. The SRM resided inside the rim and as a consequence the rim temperature was expected to rise. Based on the planned forced cooling, the transient thermal load was modelled. The ambient temperature of 22°C and the relative time dependent temperature rise of 70°C were modelled on the rim and the end cap internal faces. The convection coefficient of 50W/m^2-°C was modelled to the rim and end cap external faces. In automotive industries, generally the uniform distributed load is modelled for compliance with the SAE J2530 standard for evaluation of rims. The uniform distributed load was modelled over a 40° arc area on the outer rim faces as shown in Figure 4. The load is 1.5 times the rear axle weight of vehicle; this scaling of load compensates the effect of road bumps on the rim during the vehicle ride. Equation 1 is used to model the load condition for compliance to the SAE standard:

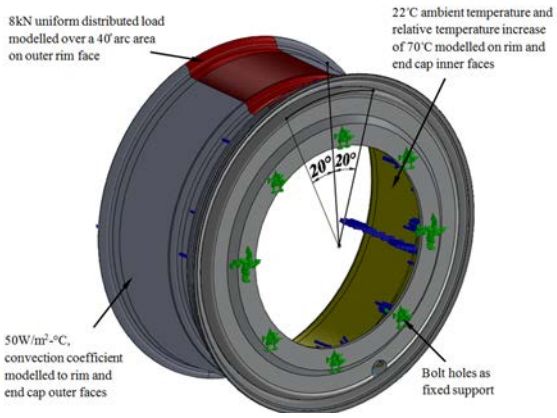

Figure 4. Rim 3 load conditions modeling

$$F = 1.5\,F' \quad (1)$$

Whereby, F is the total load required to be modelled and F' is the rear axle weight of the vehicle. The Barina Spark weight is 960kg and then 100kg is a motor weight. Using Equation 1 the total uniform distributed downwards load 8kN (towards the ground zone) on the rim is modelled over a 40° arc area on outer rim face as shown by arrows in Figure 4. The rim is subjected to cyclic loads during the vehicle travel and as a result fatigue in the rim may cause a failure. Hence the rim fatigue analysis was conducted with a compliance to the SAE J2530 standard. As per the standard, the rim is required to fulfill the minimum life cycles of 1,850,000 and possess a factor of safety (FOS) of 1.4 or more. The fatigue load was modeled fully reverse constant amplitude modelling, compressive stresses of the negative magnitude and tensile stresses of the positive magnitude are used in repetitive cycles.

2.5. Finite element results

The FE results of all five rims is summarised in Table 1 and discussions use the rim 3 figures as an example. As shown in Table 1, 59MPa and 57MPa maximum stresses were observed in the solid single piece rim 1 (11kg) and 2 (9kg) respectively. The rim 3 with the hollow end cap as shown in Figure 5, weighed 7kg, and a 164MPa maximum stress was observed. The rim 4 had a 125MPa maximum stress value and weighed 6kg. The rim 5 had a 373MPa maximum stress value and weighed 5.5kg.

Though solid in construction the rim 1 and the rim 2 showed total deformations of 1mm and 0.6mm. In contrast, the lowest deformation of 0.3mm in the downward direction was found for the rim 3. The rim 1 and the rim 2 deformed more than rim 3, as it had bolt holes near the cylindrical rim, while the rim 1 and the rim 2 had it on the central locations. The rim 4 and the rim 5 had total deflections of the magnitude 1.5mm and 5.55mm, respectively. Strain levels, as shown in Table 1, were negligible for all the rims.

S.no	Rim Description/ Mass (Kg)	Von-mises stress (MPa)	Total deformation (mm)	Total strain (mm/mm)	FOS	Minimum life cycles
1	Single piece construction positive offset with solid end cap (11kg)	59	1	0.001	1.5	100000000
2	Single piece construction zero offset with solid end cap (9kg)	57	0.6	0.001	1.5	100000000
3	**Two piece rim with hollow end cap (7kg)**	**164**	**0.3**	**0.002**	**1.5**	**24410000**
4	Five support single piece construction (6kg)	125	1.5	0.001	0.65	1553800
5	Three support single piece construction (5.5kg)	373	5.55	0.005	0.22	25000

Table 1. *Summary on evaluations of different rims*

The FOS is the ratio of material yield strength to the maximum stress level in the rim topology. The rim 4 and the rim 5 displayed a low FOS of 0.65 and 0.22 respectively. Rims 1 to 3 displayed a FOS of 1.5 as shown in Table 1. The life cycle results for all rims are shown in Table 1, for the rim 1, 2, and 3, exceeded the SAE rim life cycle requirements (SAE J2530 2009). The rim 3 had the lowest life cycle of 24410000 at the rim inner circumference, which surpassed the SAE standard requirements. These results also indicated that the rim 4 and 5 were below the recommended SAE life cycle limits.

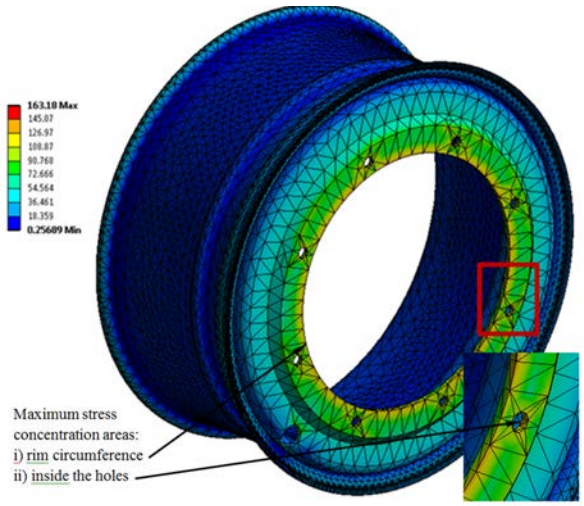

Figure 5. Rim 3 Von-mises stress concentration

Amongst compared five rims, the rim 3 had a median weight of 7kg and performed well under the modelled loads, with the lowest deflection of 0.3mm, and the maximum stress of 164MPa. The life cycle analysis also indicated that the rim 3 exceeded the SAE J2530 requirements relevant for this study. These findings indicated that the hollow end cap two piece rim weighing 7kg (rim 3) was the most suitable choice for the in-wheel SRM.

3. TYRE SIMULATIONS

3.1. Rolling resistance

Tyre when in motion has a contact with the ground surface. Both the wheel and the ground are subject to deformations and tyre springs back to the original position once the contact area is surpassed. This deformation causes the rolling resistance. Sliding between the tyre- ground and aerodynamic drag are other parameters affecting the rolling resistance. The tyre velocity is dependent on the tyre deformations, and tyre deforms every time the tyre contacts the ground surface. The contact area is called as a tyre-ground zone. As the tyre enters the ground zone, the tyre slows down, leading to the tyre circumferential compression. As there is limited sliding between the tyre and the ground in this zone, the velocity at the contact point is same as the velocity at the centre of the wheel. This is the reason for rigid wheels having higher spin speeds than pneumatic tyres under the same load. The tyre radius *R* at the ground contact is under

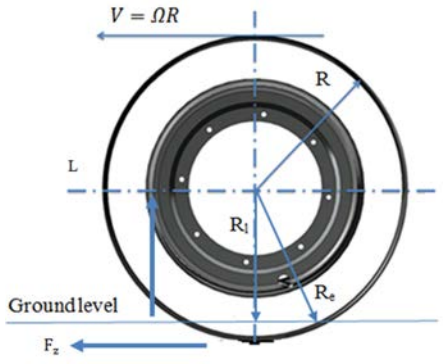

Figure 6. Tyre model

deformation R_l and tyre elastic return causes it to have the effective rolling radius of R_e. Figure 6 shows the rotating pneumatic tyre explaining all three radii, peripheral velocity, and forces acting. The tyre-ground contact leads to various changes in the tyre, affecting the rolling radius (R_e). Rolling radius is defined as the ratio of the Velocity (V) and the Angular Velocity (Ω) as shown in Equation 2 (Genta 2006):

$$R_e = V/\Omega \tag{2}$$

The rolling resistance is the resistance offered by the ground to the movement of the vehicle. Equation 3 below represents the rolling resistance:

$$F_r = -fF_z \tag{3}$$

Where, F_r is rolling resistance, f is rolling resistance coefficient (RRC) and $F_z$is force at tyre-ground contact in upward direction. In this research RRC was evaluated at normal dry environmental conditions. Radial tyres are characterised by lower vertical stiffness, leading to decreased loaded radius (R_l), but are circumferentially stiffer with rolling radius R_e values closer to rigid wheel R (Genta 2006). This leads to lower spin speeds in the contact zone. The RRC increase is non-uniform and its magnitude varies with the speed, whereby it is slow at the beginning, after which it increases at a faster rate, as given by Equation 4:

$$f = f_0 + KV^2 \tag{4}$$

Using the above Equation 4, NRR (normal rolling resistance, initially 0.12) and LRR (low rolling resistance, initially 0.07) tyres were modelled for an EV. The results depict that RRC was much smaller and changed at a lower rate with the vehicle speed increase. In the proposed in-wheel SRM, the temperature rise is expected near the tyre. This temperature rise affects the tyre rolling resistance. This is simulated by examining the correlation between the temperature and the pressure is used to establish temperature rise effects on the rolling resistance. The empirical formula provided by SAE J670e to measure the RRC accounting the influence of the inflation pressure is given by Equation 5 below (Genta 2006):

$$f = \frac{K'}{1000}\left(5.1 + \frac{5.5*10^5+90F_z}{p} + \frac{1100+0.0388F_z}{p}V^2\right) \tag{5}$$

This equation established that RRC decreased with the increase of tyre inflation pressure and temperature.

3.2. Longitudinal slip

In this section, the tyre longitudinal slip is modelled to determine the changes in drive characteristics as a consequence of the increased motor mass. When braking, a moment M_b is applied to the tyres, causing the contact zone to stretch, which leads to an increase in the radius at the point of contact to R'_e. This causes a decrease in the tyre angular velocity (Ω) at that point. During the rolling, the effective tyre rolling radius is R_e and the contact area between the ground and the tyre is compressed rather than stretched, thus shifting R_e more towards R in the range between R and R_l and leading to an increased angular velocity (Ω_0). In such conditions, it is possible to define a longitudinal slip, given by Equation 6:

$$\sigma = \Omega/\Omega_0 \tag{6}$$

The longitudinal force μ_x defines a relationship between longitudinal (F_x) and vertical forces (F_z) as shown in Equation 7:

$$\mu_x = F_x/F_z \tag{7}$$

The magnitude of longitudinal force $F_x$is modelled using the magic formula also called as a Pacejka tyre model, which provided a relationship between the longitudinal force F_x and the longitudinal slip σ, as per Equation 8:

$$\mathrm{F_x} = \mathrm{D}\sin(\mathrm{C}\tan^{-1}\{\mathrm{B}(1-\mathrm{E})(\sigma+\mathrm{S_h}) + \mathrm{E}\tan^{-1}[\mathrm{B}(\sigma+\mathrm{S_h})]\}) + \mathrm{S_v} \tag{8}$$

In this research the longitudinal force is modelled based on the car travelling on the dry road using the low rolling resistance 205/50/R17 tyre. The effects of the side force ($\mathrm{F_y}$) and wet conditions were not considered in this study. In Equation 8, B, C, D, E, $\mathrm{S_v}$, and $\mathrm{S_h}$ are six rolling coefficients dependent on the vertical load $\mathrm{F_z}$ and the angle γ. The values of these rolling coefficients are expressed as a function of coefficients b_i. The coefficient b_i values are based on data obtained by supplier for the low rolling resistance 205/50/R17 tyre. Figure 7 shows variation of the longitudinal force on a car tyre for both ICE and EV versions, with varying values of the longitudinal slip. The values σ ranged from the positive slip ($\sigma > 0$) during driving traction, zero during the free rolling ($\sigma = 0$) and the negative slip during the braking traction ($\sigma < 0$). The comparison

between the two cars established that there was slight variance in the drive characteristics of the EV when compared to the ICE car. Although these variations were negligible, it was concluded that an increase in the EV longitudinal slip tyre was due to increased mass on the tyre.

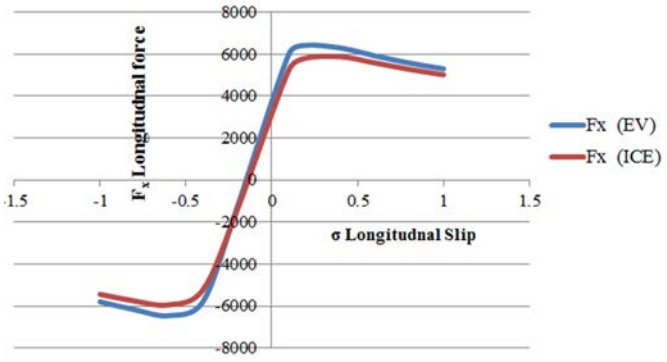

Figure 7. Longitudinal slip and force for an EV and ICE cars

4. DISCUSSION AND CONCLUSIONS

In this paper the rim and tyre were simulated for an in-wheel motor of the EV. The weight optimisation on five rim designs was condcuted using FE methods, for the structural rigidity, the thermal stability, and the life cycle assessment. Among five rims modelled in the evaluation process, the two piece hollow end cap, rim 3 was selected as it had 7kg optimal weight, 164MPa maximum stress, 0.3mm maximum deformation, 1.5 FOS and 0.02 strain. Also, the Rim 3 had 24,000,000 life cycles exceeding SAE J2530 standard minimum life cycle requirements.

The low rolling resistance increased the EV range. The RRC at different car speed was examined for LRR and NRR tyres. The comparisons concluded that the NRR tyre was less efficient than the LRR t. The effect of the inflation pressure and temperatures on the RRC was established using the SAE J670e empirical formula. The RRC decreased with the tyre inflation pressure increase (limited to the maximum allowable tyre pressure). The variation of the tyre pressure was linear with the temperature, since RRC decreased with the tyre temperature increase. Using a Pacejka's magic formula, the relationship of the longitudinal slip and the longitudinal force was modelled for the EV and the ICE. The graph plotted indicated slight variations in the EV compared to the ICE. The longitudinal force exerted by the EV was found to exceed the force exerted by the ICE car for the same value of the longitudinal slip, due to the additional motor mass.

ACKNOWLEDGMENTS

Author thanks Auto CRC for funding and supporting of EV drive train visionary project.

REFERENCES

Campbell, P. (August 2008). System Cost Analysis for an Interior Permanent Magnet Motor, Ames Laboratory Iowa State University, Ames, Iowa 50011.

Chan, C. C. (2002). The state of the art of electric and hybrid vehicles. IEEE.

Genta, G. (2006). Motor Vehicle Dynamics. Toh Tuck Link, World Scientific Publising Co. Pte. ltd.

Kulkarni, A., A. Kapoor, M. Ektesabi and H. C. Lovatt (2011). Architectural proposals for electric vehicle design. Proceedings of the ASME 2011 International Mechanical Engineering Congress and Exposition Denver, USA, ASME.

Merlin, M., G. Timelli, F. Bonollo and G. L. Garagnani (2009). "Impact behaviour of A356 alloy for low-pressure die casting automotive wheels." Journal of Materials Processing Technology **209**(2): 1060-1073.

SAE J2530 (2009). Aftermarket Wheels—Passenger Cars and Light Truck—Performance Requirements and Test Procedures. Radial test procedures SAE International.

Seaman, J. (2010). "Rare earths and clean energy: analyzing China's upper hand." Retrieved 13 October, 2011, from http://www.ifri.org/downloads/ifrinoteenergieseaman.pdf.

Wadnerkar, V. S., D. G. Tulsiram and A. D. Rajkumar (2005). "Performance Analysis Of Switched Reluctance Motor; Design, Modeling and Simulation of 8/6 Switched Reluctance Motor." Journal of Theoretical and Applied Information Technology **4**(13): 1118-1124.

Xue, X. D., K. Cheng and N. C. Cheung (2008). Selection of electric motor drives for electric vehicles. Australasian Universities Power Engineering Conference, Sydney, NSW.